Posted on Authorea 2 Sep 2020 — The copyright holder is the author/funder. All rights reserved. No reuse without permission. — https://doi.org/10.22541/au.159908941.13197198 — This a preprint and has not been peer reviewed. Data may be preliminary.

Multi-Enzyme Cascade Reaction in a Miniplant Two-Phase-System: Model Validation and Mathematical Optimization

Jens Johannsen[1], Francesca Meyer[1], Claudia Engelmann[1], Andreas Liese[1], Georg Fieg[1], Paul Bubenheim[1], and Thomas Waluga[1]

[1]Hamburg University of Technology

September 2, 2020

Abstract

Biotechnological application of multiple enzymes in different phases for target compounds synthesis poses a significant challenge for industrial process development. At the same time, a growing demand for natural flavors and fragrances opens up possibilities for novel biotechnological processes to replace current chemical synthesis routes, with additional advantages such as avoiding harsh reaction conditions and toxic chemicals, and less by-products in the system. Within complex biotechnological processes, the key for unfolding their industrial application potential in bioprocess engineering lies in their mathematical modeling. In this contribution, a multi-enzyme cascade reaction in a two-phase system implemented in a miniplant-scale reactor setup is mathematically modeled for the example of the flavoring agent cinnamyl cinnamate. Using our validated model and a mathematical optimization tool based on a genetic algorithm, optimization runs are performed to demonstrate the potential of computer-aided process development for complex biotechnological processes.

Text

Introduction

The worldwide market for flavors and fragrances generates a 30 billion US-$ revenue volume per year, and grows at a 5 % annual rate. Natural flavor production is of increasing importance, predominantly in Europe and North America. The U.S. Food & Drug Administration defines natural flavors as those deriving their chemicals from animal or plant sources, as opposed to artificial flavors that use synthetic chemicals in the production process.

Industrial biotechnology can fulfill naturality prerequisites through novel, sustainable processes. At the same time, its potential to replace current chemical synthesis routes remains controversial across different fields of study such as the production of specialty and fine chemicals. Here, a promising approach to the synthesis of flavors and fragrances is the development of *in vitro* multi-enzyme cascade reactions. These combine the benefits of enzymatically catalyzed reactions (e.g. high selectivity, mild reaction conditions) with the concept of process integration. In literature, cascade reactions with up to ten reaction steps and eight enzymes have been successfully established, albeit usually limited to the application in an aqueous phase. Few examples show the application in both aqueous and organic phases: they, however, make use of process integration (extraction steps) solely in order to enhance reaction turnover, without implementing additional reaction steps in the organic phase. In previous papers, our research group conclusively proved the applicability of multi-enzyme cascade reactions in a multiphase system for the production of specialty chemicals through the example of cinnamyl cinnamate with integrated cofactor regeneration and integrated intermediate extraction. As a consequent step towards production-scale process development, within this line of research we successfully implemented a continuous production process for the flavoring agent cinnamyl cinnamate in a three liter miniplant reactor setup.

Posted on Authorea 2 Sep 2020 — The copyright holder is the author/funder. All rights reserved. No reuse without permission. — https://doi.org/10.22541/au.159908941.13197198 — This a preprint and has not been peer reviewed. Data may be preliminary.

Cinnamyl cinnamate is extracted as a natural component from Balsam of Peru, and used as a flavoring agent in cosmetic products and perfumes. Currently, two main chemical production processes are in use: styrene oxidative carbonylation with carbon monoxide, oxygen and aliphatic alcohols in the presence of palladium and sodium propionate, or cinnamic aldehyde synthesis in absolute ether with aluminum ethylate. Contrary to the conventional chemical approach, in this study we investigate an innovative production process for cinnamyl cinnamate that fits the criteria of both the U.S. Department of Health and Human Services and the European Union for labelling the product as a "natural flavor".

An important requirement to scale new production processes up for industrial application from an economic and/or ecological point of view is the possibility of a mathematical description of said process for continuous process control and development. However, due to the use of various enzymes and multiple phases, the mathematical description of complex biotechnological processes such as multi-enzyme cascade reactions constitutes an obstacle to biotechnological process development. Therefore, this study takes on the challenge of introducing a mathematical model to describe a complex biotechnological production process implemented in a miniplant. Our model is implemented in Aspen Custom Modeler® V8.8 (Aspen Technology, Inc., U.S.A.), and validated using experimental data obtained from the miniplant. In this study, we present the cinnamyl cinnamate-producing multi-enzyme cascade reaction sequence and discuss our mathematical model as well as experimental results for the miniplant. Furthermore, a mathematical optimization tool is used to perform simulation runs with the validated model, while simultaneously varying the process conditions to find optimal process operating windows, thereby proving the benefits of computer-aided process development in biotechnology.

Process Description

As the first step of process development towards a potential industrial application, the multidisciplinary studies and laboratory-scale analyses conducted by our research group and presented in previous peer-reviewed papers, resulted in the *in vitro* multi-enzyme cascade reaction sequence for the production of cinnamyl cinnamate from cinnamyl aldehyde in a multiphase system (Figure 1).

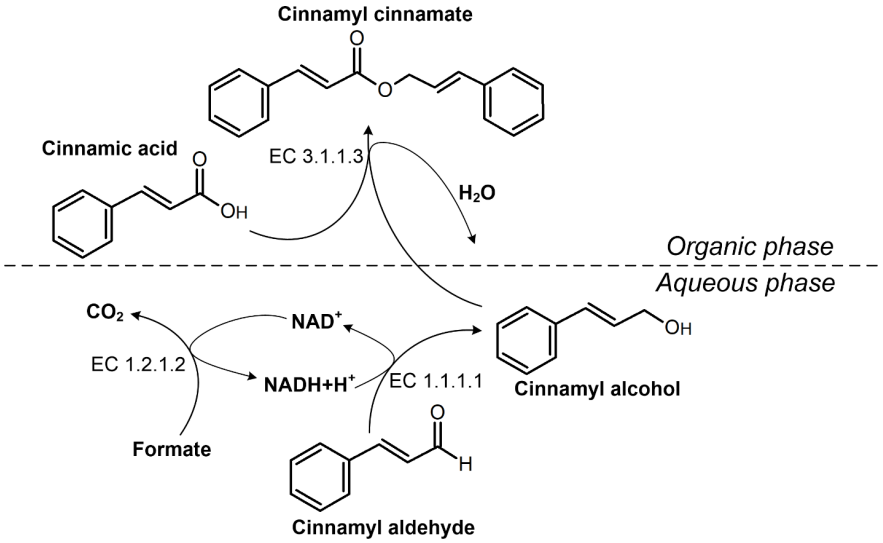

Figure 1. Multi-enzyme cascade reaction sequence for the production of cinnamyl cinnamate from cinnamyl aldehyde with integrated co factor regeneration and in situ intermediate extraction in a two-phase system.

An alcohol dehydrogenase (ADH) converts cinnamyl aldehyde to cinnamyl alcohol in a buffer phase (0.1 M potassium phosphate buffer at pH 8.0) using the cofactor NADH. Integrated cofactor regeneration within this cascade reaction sequence is ensured through addition of a formate dehydrogenase (FDH) converting

Posted on Authorea 2 Sep 2020 — The copyright holder is the author/funder. All rights reserved. No reuse without permission. — https://doi.org/10.22541/au.159908941.13197198 — This a preprint and has not been peer reviewed. Data may be preliminary.

formate to CO_2 under NAD^+ consumption. After *in situ* extraction of the intermediate cinnamyl alcohol with xylene as an organic solvent and cinnamic acid addition, the lipase Novozym® 435 performs an esterification reaction in the organic phase to synthesize cinnamyl cinnamate and water. This process has successfully been established in both the laboratory and the miniplant.

Figure 2 shows the flow chart of the miniplant used for this three-enzyme cascade reaction. The two cofactor-coupled dehydrogenases are immobilized on silica particles according to Engelmann *et al.*and placed in a two-liter continuously operated stirred tank reactor tempered to 30 °C, equipped with a SpinChem® RBR S2 rotating bed reactor (SpinChem AB, Umeå, Sweden), spinning at 400 rpm (figure 2, A). A buffer tank is used for the organic phase and for cinnamic acid feeding (figure 2, B). According to the principles of process integration, the extraction step connects both phases as they are mixed and immediately separated in one apparatus, a CINC CS 50 extractive centrifuge (CINC Deutschland GmbH & Co. KG, Brakel, Germany) (figure 2, C). For the final esterification reaction step, the cinnamic acid- and alcohol-loaded xylene phase is subsequently pumped through a fixed bed reactor, containing 12.8 g of Novozym®435 and tempered to 60 °C according to the enzyme provider's information (figure 2, D).

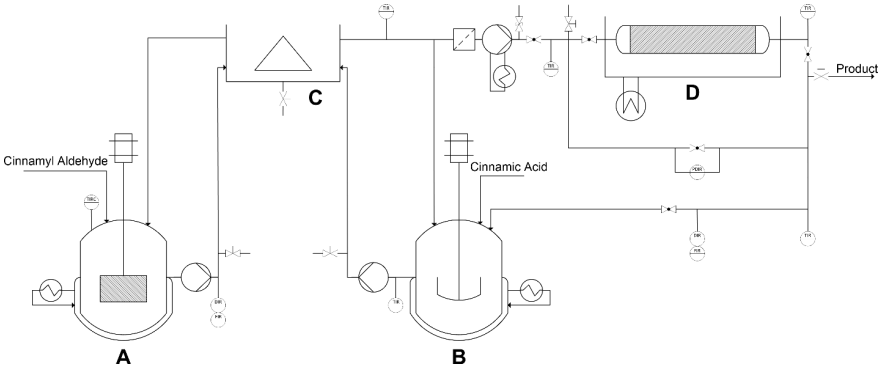

Figure 2. Flow chart of the miniplant consisting of a continuously stirred tank reactor (CSTR) (A), a buffer tank (B), an extractive centrifuge (C) and a fixed bed reactor (D).

Mathematical model

In order to simulate the multi-enzyme cascade reaction sequence in the miniplant, a customized mathematical model is developed and solved in Aspen Custom Modeler® V8.8 (Aspen Technology, Inc.) using an equation-oriented approach for simulating. As shown in figure 3, this model is divided into three sub-models: aqueous phase, phase interface, and organic phase. These sub-models are connected through differential mass balance equations for each component. The reaction kinetics used for the mathematical modeling of each enzyme have been obtained through kinetic measurements.

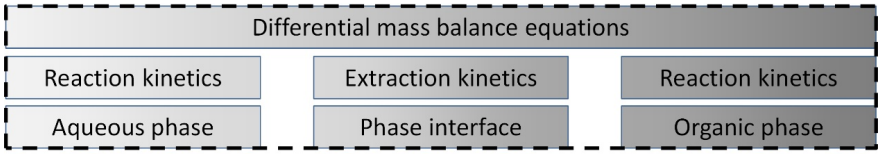

Figure 3. Schematic structure of the model for the miniplant as implemented in Aspen Custom Modeler®.

Aqueous phase

A bi-bi mechanism with competitive inhibition for both the ADH-catalyzed reaction of cinnamyl aldehyde (CAL) to cinnamyl alcohol (COH) and the FDH-catalyzed reaction of formate to CO_2 are implemented in

Posted on Authorea 2 Sep 2020 — The copyright holder is the author/funder. All rights reserved. No reuse without permission. — https://doi.org/10.22541/au.159908941.13197198 — This a preprint and has not been peer reviewed. Data may be preliminary.

the model according to kinetic analyses, describing the ADH reaction rate according to equation (1) and the FDH reaction rate according to equation (2). The corresponding values for the constants are listed in table 1.

$$v_{\mathrm{ADH}} = \frac{v_{max,ADH} \bullet ([\mathrm{CAL}] \bullet [\mathrm{NADH}])}{K_{m,CAL} \bullet K_{m,NADH+H^+} \bullet \left(1 + \frac{[\mathrm{COH}]}{K_{I,COH}}\right) + K_{m,\mathrm{NADH}} \bullet [\mathrm{CAL}] + K_{m,CAL} \bullet [\mathrm{NADH}] \bullet \left(1 + \frac{[COH]}{K_{I,COH}}\right) + [\mathrm{CAL}] \bullet [\mathrm{NADH}]} \quad (1)$$

$$v_{\mathrm{FDH}} = \frac{v_{max,FDH} \bullet \left(\left[\mathrm{NAD^+}\right] \bullet [\mathrm{formate}]\right)}{K_{m,NAD} \bullet K_{m,formate} \bullet \left(1 + \frac{[\mathrm{NADH}]}{K_{I,\mathrm{NADH}}}\right) + K_{m,formate} \bullet \left[\mathrm{NAD^+}\right] + K_{m,\mathrm{NAD^+}} \bullet [\mathrm{formate}] \bullet \left(1 + \frac{[\mathrm{NADH}]}{K_{I,\mathrm{NADH}}}\right) + [\mathrm{formate}] \bullet \left[\mathrm{NAD^+}\right]} \quad (2)$$

Table 1. Kinetic parameters of the ADH and FDH catalyzed reactions in the aqueous phase.

Parameter	Unit	Value
$v_{max,ADH}$	[U/mg$_{enzyme}$]	3.49 ± 1.53
$K_{m,CAL}$	[mM]	0.39 ± 0.20
$K_{m,NADH}$	[mM]	0.08 ± 0.07
$K_{I,COH}$	[mM]	0.04 ± 0.03
$v_{max,FDH}$	[U/mg$_{enzyme}$]	0.46 ± 0.07
K_{m,NAD^+}	[mM]	0.04 ± 0.02
$K_{m,formate}$	[mM]	10.14 ± 6.67
$K_{I,NADH}$	[mM]	0.27 ± 0.42

The kinetic equations (1) and (2) describe the reaction rates of free enzymes. During the immobilization process, a decrease in enzyme activity can be observed and is described by an efficiency factor η_{eff}. Remaining enzyme activity after immobilization for both FDH and ADH was determined to be 4 % of the respective free enzyme activity. Additionally, as described in literature, a loss of activity over time was observed for the FDH, significantly affecting the reaction rates. This time-dependent activity loss reaches values up to 68 % and is described in the model by the deactivation factor f_{deac}. The effective reaction rates for the dehydrogenases can be obtained after multiplying the respective kinetic equations with the enzyme mass, while considering the aforementioned activity losses, resulting in equation (3) for the ADH and equation (4) for the FDH respectively.

$$v_{eff,\ ADH} = f_{\mathrm{deac}} \bullet \eta_{eff,ADH} \bullet v_{\mathrm{ADH}} \bullet m_{\mathrm{ADH}} \quad (3)$$

$$v_{eff,\ FDH} = \eta_{eff,FDH} \bullet v_{\mathrm{FDH}} \bullet m_{\mathrm{FDH}} \quad (4)$$

As expected due to the application of a phosphate buffer, experimental results showed auto-oxidation of the cofactor NADH over time, as previously reported in literature. In order to model the reaction system as precisely as possible, the auto-oxidation of NADH was measured at wavelengths of $\lambda_1 = 340$ nm and $\lambda_2 = 292$ nm in a time range of 48 hours using a VWR$^{\mathrm{TM}}$ UV-1600PC Spectrophotometer. Additionally, absorption values at $\lambda_3 = 260$ nm increased analogous to NADH-oxidation during these experiments, indicating that NADH is oxidized to NAD^+. In our mathematical model it is therefore assumed, that NADH auto-oxidizes to NAD^+. The resulting NADH-oxidation for this system is described through a function of

Posted on Authorea 2 Sep 2020 — The copyright holder is the author/funder. All rights reserved. No reuse without permission. — https://doi.org/10.22541/au.159908941.13197198 — This a preprint and has not been peer reviewed. Data may be preliminary.

exponential decay as shown in equation (5):

$$\frac{d[\mathrm{NADH}]_{\mathrm{oxidation}}}{\mathrm{dt}} = [\mathrm{NADH}]_{t-1} \bullet \left(1 - 0.66 \bullet e^{-0.00179 \bullet t}\right). \quad (5)$$

Miniplant experiments showed precipitation of the components cinnamic acid, aldehyde, and alcohol from the liquid phase, because their concentration exceeded the saturation concentration. Especially the low water saturation concentration of cinnamic acid led to precipitation. In order to be able to simulate substance precipitation and dissolution in the aqueous phase and thus achieve a higher model depth, a storage term$\dot{n}_{\mathrm{precipitation,i}}$ is introduced for any given component i. In every time step of the dynamic simulation, the concentration of each component in the aqueous phase is compared to the saturation concentration of that same component. If the concentration exceeds the saturation concentration, the overlap is stored in the storage term, from which it can dissolute again at lower concentrations.

The mass balance of each component in the aqueous phase is therefore described through differential equations in dependency on the reactions of the respective enzymes, the feed streams, mass transfer to the organic phase, and the precipitated amount in each time step. Equation (6) shows the generalized form of the mass balance for any given component i in the volume specific form. Equations (7) and (8) show the modified forms of the mass balance for the cofactors NADH and NAD^+ respectively, considering the auto-oxidation of NADH instead of the non-existing precipitation of the cofactors.

$$\frac{d[i]}{\mathrm{dt}} = \pm\, v_{eff,FDH} \pm\, v_{eff,ADH} + \dot{n}_{feed,i} - \dot{n}_{transfer,i} \pm \dot{n}_{precipitation,i} \quad (6)$$

$$\frac{d[NADH]}{\mathrm{dt}} = +\, v_{eff,FDH} - v_{eff,ADH} + \dot{n}_{NADH,feed} - \dot{n}_{NADH,transfer} - \dot{n}_{NADH,oxidation} \quad (7)$$

$$\frac{d[\mathrm{NAD^+}]}{\mathrm{dt}} = -\, v_{eff,FDH} + v_{eff,ADH} + \dot{n}_{\mathrm{NAD^+},feed} - \dot{n}_{\mathrm{NAD^+},transfer} + \dot{n}_{NADH,oxidation} \quad (8)$$

Phase interface

The mass transfer at the phase interface is important, in that it affects the concentrations of all components in both phases, thereby influencing all three enzymatic reactions. Experimental results show that the mass transfer rate of all components is significantly higher than the reaction rates of all three enzymes. Therefore, the assumption of instantaneous mass transfer seems reasonable: this leads to a concentration distribution between the two phases according to the partition coefficient for each component i as described according to equation (9).

$$P_i = \frac{[i]_{\mathrm{organic\ phase}}}{[i]_{\mathrm{aqueous\ phase}}} \quad (9)$$

The partition coefficients were determined in concentration ranges of 0.02 - 1000 mM in triplets and are listed in table 2. As expected, the partition coefficients proved to be concentration-independent.

Table 2. Partition coefficients of all components in the two phase system.

Component	Unit	Partition coefficient
CAC	[-]	23.3
CAL	[-]	7

Posted on Authorea 2 Sep 2020 — The copyright holder is the author/funder. All rights reserved. No reuse without permission. — https://doi.org/10.22541/au.159908941.13197198 — This a preprint and has not been peer reviewed. Data may be preliminary.

Component	Unit	Partition coefficient
CCI	[-]	1000
COH	[-]	5.6
NAD^+	[-]	0
NADH	[-]	0

Analogous to the aqueous phase, component precipitation is described with storage terms for the extractive centrifugation step. Additionally, during this step, each one of the two phases is saturated with its counterpart. The temperature in the extractive centrifuge influences the productivity of the final reaction step by affecting water saturation concentration in the organic phase, as described in previous studies. Therefore, the linear temperature-dependent water saturation concentration of the organic phase is implemented in the model according to equation (10).

$$w_{water-organic} = 0.0015 \bullet T_{\text{centrifuge}} + 0.0081 \quad (10)$$

Organic phase

The immobilized-lipase-filled fixed bed reactor for the esterification reaction is modeled as a cascade of σ CSTR reactors according to equation (11). For each CSTR j, a mole flow$\dot{n}_{\text{CSTR,j,i}}$ is defined which contains the concentrations of all cinnamyl derivatives for the subsequent CSTR j+1. A deactivation of Novozym®435 was not noted over time; therefore no time-dependent deactivation constant is implemented. Due to temperature variations between the extraction step and the fixed bed reactor, a temperature-dependent concentration change is implemented through a temperature-dependent change in density ϱ of the organic phase. Since component precipitation in the organic-phase cycle was not noted due to the high saturation concentrations of the cinnamyl derivatives, no storage term is implemented in this sub-model. Based on kinetic measurements, the lipase reaction rate is described according to a bi-bi mechanism with substrate excess inhibition of cinnamic acid (CAC) for the present reaction system. Equation (12) shows the lipase reaction rate as implemented in the model, and the corresponding parameters are described in table 3.

$$\dot{n}_{CSTR,j,i} = c_{CSTR,j-1,i} \bullet v_{\text{lipase}} \bullet \frac{m_{\text{lipase}}}{\sigma} \quad (11)$$

$$v_{\text{lipase}} = \frac{v_{max,lipase,forward} \bullet \left([\text{COH}] \bullet [\text{CAC}] - \frac{[H_2O] \bullet [\text{CCI}]}{K_{\text{eq}}}\right)}{K_{I,CAC} \bullet K_{m,COH} + K_{m,COH} \bullet [\text{CAC}] \bullet (1 + \frac{[\text{CAC}]}{K'_{I,CAC}}) + K_{m,CAC} \bullet [\text{COH}] + [\text{COH}] \bullet [\text{CAC}] + \frac{v_{max,lipase,forward}}{v_{max,lipase,reverse}} \bullet \frac{K_{m,H2O} \bullet [\text{CCI}]}{K_{\text{eq}}} + \frac{v_{max,lipase,forward}}{v_{max,lipase,reverse}} \bullet \frac{K_{m,CCI} \bullet [H_2O]}{K_{\text{eq}}} + \frac{v_{max,lipase,forward}}{v_{max,lipase,reverse}} \bullet \frac{[\text{CCI}] \bullet [H_2O]}{K_{\text{eq}}}} \quad (12)$$

Table 3. Kinetic parameters of the lipase catalyzed esterification reaction in the organic xylene phase.

Parameter	Unit	Value
$v_{\text{max,lipase,forward}}$	[U/mg_{enzyme}]	6.3 ± 1.2
$v_{\text{max,lipase,reverse}}$	[U/mg_{enzyme}]	14.8 ± 2.8
$K_{\text{m,CAC}}$	[mM]	1.4 ± 0.3
$K_{\text{m,COH}}$	[mM]	2.8 ± 0.5
$K_{\text{m,H2O}}$	[mM]	0
$K_{\text{m,CCI}}$	[mM]	0.8 ± 0.2

Posted on Authorea 2 Sep 2020 — The copyright holder is the author/funder. All rights reserved. No reuse without permission. — https://doi.org/10.22541/au.159908941.13197198 — This a preprint and has not been peer reviewed. Data may be preliminary.

Parameter	Unit	Value
$K_{I,CAC}$	[mM]	13.7 ± 2.6
$K_{I,H2O}$	[mM]	252.9 ± 48.1
K_{eq}	[-]	2.6 ± 0.5

Model validation

The mathematical model described in this work was developed based on experimental data from our multi-enzyme cascade reaction (Figure 1) during the first step of laboratory-scale process development. Our model aims to simulate the cinnamyl cinnamate production process in the miniplant introduced in figure 2, thereby making time- and cost-intensive experiments for process optimization obsolete. Therefore, the model is to be used for mathematical optimization. Prior to process simulation and optimization, however, our model needs to be validated using independent experimental data from the miniplant as the consequent second step of process development. Since the developed mathematical model is designed to perform dynamic simulations, the start-up phase of the reactor setup has to be included in the validation process.

All experiments for model validation were performed in the miniplant described in figure 2 in the previous chapter. 500 ml of a 0.1 M potassium phosphate buffer at pH 8.0 were used in the continuously stirred tank reactor (figure 2, A), tempered to 30 °C. This device is equipped with a SpinChem® reactor, spinning at 400 rpm and containing 21.3 mg of immobilized ADH and 6.6 mg of immobilized FDH. 250 ml/min are pumped within the water-based cycle through the extractive centrifuge (figure 2, C), thereby connecting the two cycles. The organic cycle consists of 500 ml of xylene provided in the buffer tank (figure 2, B), 100 ml/min of which are pumped via the extractive centrifuge through the fixed bed reactor (figure 2, D) filled with 12.8 g of Novozym®435 and tempered to 60 °C. Six different experiments were performed with varying starting concentrations, to validate our mathematical model using a broad range of experimental data. Table 4 shows the supplied starting concentrations of the educts for all six experiments, as well as the achieved molar yield of CCI after 54 hours of operation with respect to the CAL starting concentration, calculated according to equation (13).

$$Y_{CCI,t} = \frac{n_{CCI,t}}{n_{CAL,t=0}} \quad (13)$$

Table 4. Starting concentrations of educts and CCI yield for the six experiments performed in the miniplant.

Experiment	NADH [mM]	CAL [mM]	Formate [mM]	CAC [mM]	$Y(CCI)_{54h}$ [%]
1	3.2	6.9	324.0	24.3	14.1
2	3.5	8.8	328.0	56.3	24.9
3	3.5	6.8	328.0	94.7	22.8
4	5.0	6.9	350.0	64.3	21.6
5	1.5	0.7	291.0	101.7	16.5
6	0.5	3.1	97.6	24.3	15.2

During the experiments, samples were taken from both phases and analyzed in a Perkin Elmer Clarus 500® (PerkinElmer Inc., U.S.A.) gas chromatograph equipped with a 30 m SLB SUPELCO® (Supelco, Inc., U.S.A.) column with a 0.25 mm x 0.25 µm cross section, thus generating concentration profiles of all components over time. Exemplary for our experimental results, figure 4 shows the concentration profiles of the intermediate COH and the final product CCI in the organic phase of experiment 2 as well as the corresponding simulated values using the mathematical model described in the previous chapter. The experiment shown in figure 4 has a total duration of 80 hours: during the first 65 h, the aqueous cycle is running without the

Posted on Authorea 2 Sep 2020 — The copyright holder is the author/funder. All rights reserved. No reuse without permission. — https://doi.org/10.22541/au.159908941.13197198 — This a preprint and has not been peer reviewed. Data may be preliminary.

organic cycle, allowing for a separate evaluation of the reactions as well as sufficient intermediate formation leading to a clearer concentration profile in the later connected organic cycle.

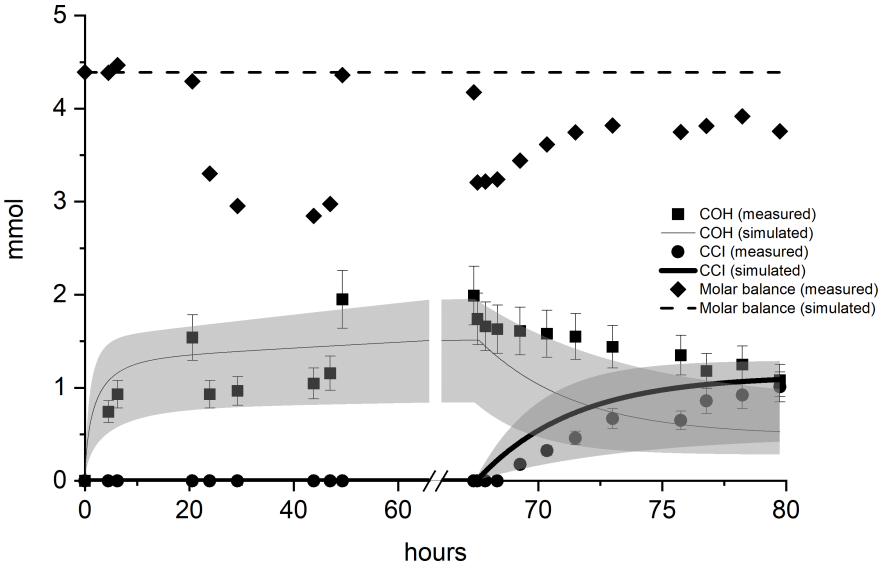

Figure 4. Experimental and simulated data of experiment number 2 for model validation.

In figure 4, the squares and circles indicate the measured concentrations of COH and CCI respectively. The continuous line shows the simulated values for COH concentration, surrounded by a shaded area which indicates concentration value ranges induced by the standard deviation ranges of the kinetic parameters. The dotted line indicates the simulated values for CCI, again surrounded by a value range induced by the standard deviations obtained in the kinetic parameters determination. The dashed line shows the overall molar balance equation which is unchanged during the course of a simulation due to the equimolar reactions, while the experimentally measured molar balances are indicated by the diamonds. The overall molar balance includes the components CAL and CAC.

As can be seen in figure 4, the intermediate concentration of COH increases for the first 65 h and then decreases after the organic cycle is connected and the lipase performs the esterification reaction, leading to a constant increase in CCI concentration. The mean deviations of the experimental values from the simulated values are 26.7 % and 20.8 % for COH and CCI respectively. CCI shows good agreements throughout the experiment, while COH concentrations vary towards the end of the experiment. Deviations of experimental and simulated COH values can also be observed during the first phase of the experiments at around 2000 min. In both cases, these deviations can be explained with the experimentally measured overall molar balance, which does not mathematically add up during those measurements. Especially in the last 800 min of the experiment, the experimentally determined molar balance varies: this can be due to dead volume in the organic cycle containing xylene, leading to a dilution of the samples or precipitation of the components CAL, COH, or CAC.

Throughout all six experiments we simulated for model validation, the mean deviation reached values of 26.0 % and 22.6 % for COH and CCI respectively. In literature, mathematical models for such complex multi-enzyme processes across phase boundaries in miniplant-scale and continuous operation cannot be found to the best of our knowledge. Examples of enzyme-based process modeling and simulation exist that do not validate the model with independent experimental data, or their validation is based on qualitative agreement between experimental and simulated values. Few examples exist for less complex and less time intensive reaction sequences that allow for a quantitative evaluation, giving deviations in the range of approximately 25 %, or of above 30 % for dynamic simulations. In the reactive zone filled with Novozym®435 of a technical-scale

Posted on Authorea 2 Sep 2020 — The copyright holder is the author/funder. All rights reserved. No reuse without permission. — https://doi.org/10.22541/au.159908941.13197198 — This a preprint and has not been peer reviewed. Data may be preliminary.

reactive dividing wall column operated with one reaction, Egger observed concentration deviations between experiments and simulations of up to 20 %. Therefore, it can be stated that the simulated values throughout all six experiments presented in this work lie in good agreement with the experimental results, proving the applicability of our model to the reactor setup. Using our validated model, process optimization can now thus be conducted without the need for further experimental runs.

Process optimization

With the help of our simulation model described in the previous chapter, computational process optimization methods can now be used to mathematically optimize process conditions and find the optimal operating windows for the multi-enzyme cascade reaction sequence implemented in our miniplant. More specifically, the Institute of Process and Plant Engineering at Hamburg University of Technology has developed the multi-objective process optimization tool "Advanced Process Optimizer" (Adv:PO V0.7), which can be coupled with flow sheet simulator tools such as Aspen Custom Modeler® . The Adv:PO makes use of a genetic algorithm and has been successfully applied to various chemical and biotechnological processes. The implementation of this tool, together with our novel mathematical model, allows for in-depth analysis and process improvement of the multi-enzyme cascade reaction sequence to find optimal operating conditions.

During the optimization run, process variables, i.e. the concentrations of each component, are varied between physically defined limits. Such constraints are determined by component solubility and by the capacity of the miniplant. Multi-objective mathematical functions are defined in order to find the optimal solutions for any experimental variable of the cascade reaction. In this paper we focus exemplarily on presenting our results for maximizing CCI space-time yield in steady-state operation, while at the same time minimizing the amount of the costly cofactors NADH and NAD^+. Such focus will broaden the single-criterion-approach of increasing product space-time yield by the economic factor of avoiding unnecessary amounts of costly substances. The objective functions f_1 and f_2 in equation (14) and (15) represent the maximizing of CCI space-time yield and the minimizing of the cofactor input. They are complemented by physical constraints. As shown in equation (16), the concentration for each component must range within physically reasonable values. Moreover, all dimensions, flow rates, temperatures, and kinetic parameters must stay constant throughout the optimization run. Possible trivial solutions of zero are not accepted: a minimum CCI space-time yield of 0.1 mmol/(l[?]h) is set as a constraint for valid solutions.

$$\max f_1 = \max\left(\dot{n}_{CCI,out}\right) = \max f(v_{eff,ADH}, v_{\mathrm{FDH}}, v_{\mathrm{Lipase}}) \quad (14)$$

$$\min f_2 = \min\left(n_{Co-factor}\right) = \min f(c_{\mathrm{NAD^+}},\ c_{\mathrm{NADH}},\ V) \quad (15)$$

$$0 \leq c_i \leq c_{\mathrm{solubility}} \quad (16)$$

This results then in a Pareto front representing a set of optimal solutions, each one being a trade-off of the objective functions whereby no other solution can satisfy both objective functions better. Exemplarily for these results, figure 5 shows a multi-objective optimization run to increase the CCI space-time yield while decreasing the cofactor concentration after 50, 200, and 300 generations respectively: as can be seen in figure 5, 200 generations are sufficient as no significant improvement is obtained even when increasing the generation number.

Posted on Authorea 2 Sep 2020 — The copyright holder is the author/funder. All rights reserved. No reuse without permission. — https://doi.org/10.22541/au.159908941.13197198 — This a preprint and has not been peer reviewed. Data may be preliminary.

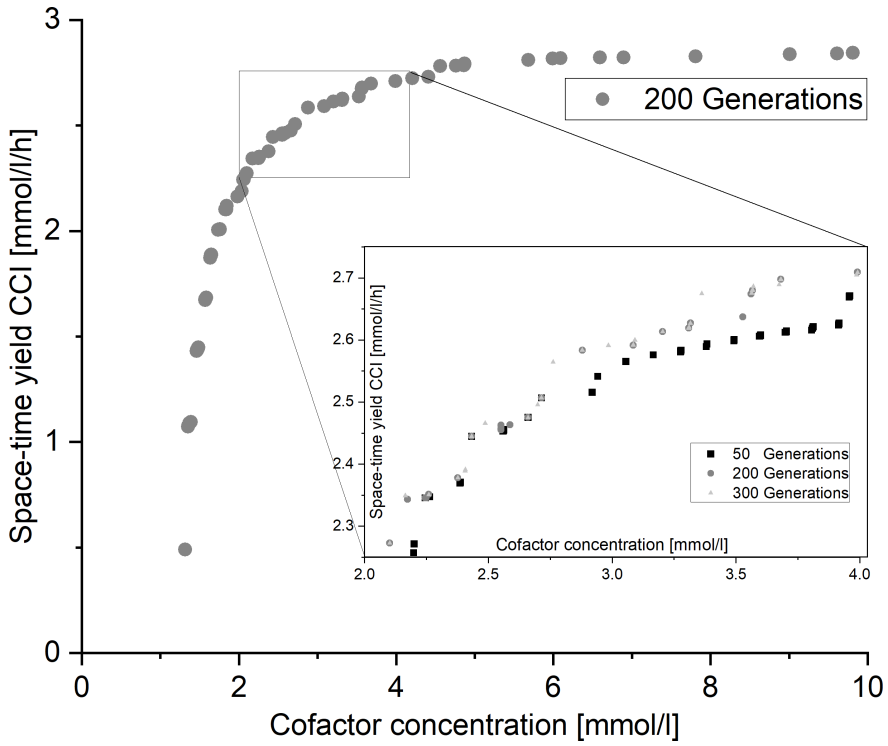

Figure 5. Pareto front of a multi-objective optimization of product flow and cofactor concentration in the cascade reaction sequence with varying generation number.

The optimal values shown in figure 5 vary from 1.3 mmol/l to 9.8 mmol/l for cofactor concentration and 0.49 mmol/(l[?]h) to 2.84 mmol/(l[?]h) for CCI space-time yield respectively. Moreover, our results identified a suitable operating window, as the CCI space-time yield rate significantly increases with a higher cofactor concentration. This remains true up to a value of approximately 4.2 mmol/l, after which the space-time yield difference is smaller than 1 % with increasing cofactor concentration. The lower operating window frame can be set according to a usual space-time yield value of 1 mmol/(l[?]h) for industrial biotechnological processes and to a corresponding cofactor concentration of 1.4 mmol/l, thereby framing the most promising operating window with regard to the aforementioned two objectives.

Such optimization runs can now be performed for multiple experimental conditions and objectives, allowing for a profound understanding of the multi-enzyme cascade reaction sequence and the production process of CCI in the miniplant without the need for cost- and time-intensive experiments. To the best of our knowledge, multi-objective mathematical process optimization has not yet been applied to complex multi-enzyme cascade reactions in a miniplant-scale reactor setup.

Conclusion and Outlook

The world-wide growing demand for natural flavors poses a chance for enzyme-based production processes to be implemented to specialty and fine chemicals industry. *In vitro* multi-enzyme cascade reactions are a promising part of such novel, enzyme-based approaches, in that they present a chance for process integration. Within our research group, a three-enzyme cascade reaction sequence with integrated cofactor regeneration and integrated intermediate extraction in a two-phase system has been successfully established and scaled up for application in a miniplant at the example of the ester cinnamyl cinnamate. Due to their high complexity compared to conventional chemical synthesis routes, however, such enzyme-based processes are difficult to mathematically describe. On the other hand, mathematical modeling is an important prerequisite for the industrial application of novel production processes.

Posted on Authorea 2 Sep 2020 — The copyright holder is the author/funder. All rights reserved. No reuse without permission. — https://doi.org/10.22541/au.159908941.13197198 — This a preprint and has not been peer reviewed. Data may be preliminary.

Therefore, in this contribution the authors introduce an Aspen Custom Modeler® - implemented mathematical model to describe the aforementioned complex biotechnological production process for a miniplant-scale reactor setup. Here, sub-models for each thermodynamic phase and for the integrated extraction step respectively are connected through differential mass balance equations, resulting in one holistic mathematical model describing the cascade reaction. In this study, successful validation of the model with independent experimental data obtained from the miniplant is presented for the first time. Using this validated model, multi-objective mathematical optimization runs were performed with the in-house-developed optimization tool Adv:PO. As a result, the authors can now identify optimal process operating windows for any given multi-objective function within the cascade reaction. The Pareto-optimal dependency of cofactor concentration on cinnamyl cinnamate space-time yield is analyzed and shown in this work as a representative example for such optimization results, obtaining a suitable cofactor concentration range of 1.4 mmol/l to 4.2 mmol/l.

Future research will now further investigate the optimal operating settings for the miniplant-scale production process. Specifically, integration of the product separation step will be the focus of our work: promising results for cinnamyl cinnamate separation from the product mixture were already achieved using annular chromatography. Incorporating the downstream process into the mathematical model for process optimization will show the full potential of this novel process specifically, and the benefits of applying mathematical modeling and optimization to biotechnology in general.

Acknowledgments

The authors thank the Deutsche Forschungsgemeinschaft (German Research Foundation) for funding this project (DFG WA 3957/1-1 & DFG BU 3409/1-1), and Novozymes® for the generous donation of Novozym®435.

Notation

ADH = Alcohol dehydrogenase

CAC = Cinnamic acid

CAL = Cinnamyl aldehyde

CCI = Cinnamyl cinnamate

COH = Cinnamyl alcohol

CSTR = Continuously Stirred Tank Reactor

FDH = Formate dehydrogenase

f = Objective function for Optimization

f_{deac} = Deactivation factor of FDH [-]

h = Hour

i = Index referring to any component of the system

j = Index referring to any CSTR in the CSTR-cascade

K_{eq} = Equilibrium constant [-]

K_I = Inhibition constant [mM]

K_m = Michaelis-Menten constant [mM]

l = Liter

m = Mass [mg]

$\dot{n}$ = Mole flow [mmol/min]

Posted on Authorea 2 Sep 2020 — The copyright holder is the author/funder. All rights reserved. No reuse without permission. — https://doi.org/10.22541/au.159908941.13197198 — This a preprint and has not been peer reviewed. Data may be preliminary.

n = Mole number [mmol]

$\dot{n}_{\text{feed,i}}$ = Feed of component i into the aqueous phase [mM/min]

$\dot{n}_{\text{precipitation,i}}$ = Storage term in the aqueous phase of component i [mM/min]

$\dot{n}_{\text{transfer,i}}$ = Mass transfer of component i to the organic phase [mM/min]

P = Partition coefficient [-]

T = Temperature [°C]

t = time [min]

V = Volume [m^3]

v = Reaction rate [U/mg_{enzyme}]

v_{eff} = Effective reaction rate [U]

v_{max} = Maximum reaction rate [U/mg_{enzyme}]

w = Mass fraction [g/g]

Y = Yield [mol/mol]

η_{eff} = Efficiency factor of enzyme immobilization [-]

ϱ = Density [kg/m^3]

σ = Number of CSTR reactors modeled for the fixed bed reactor

Literature

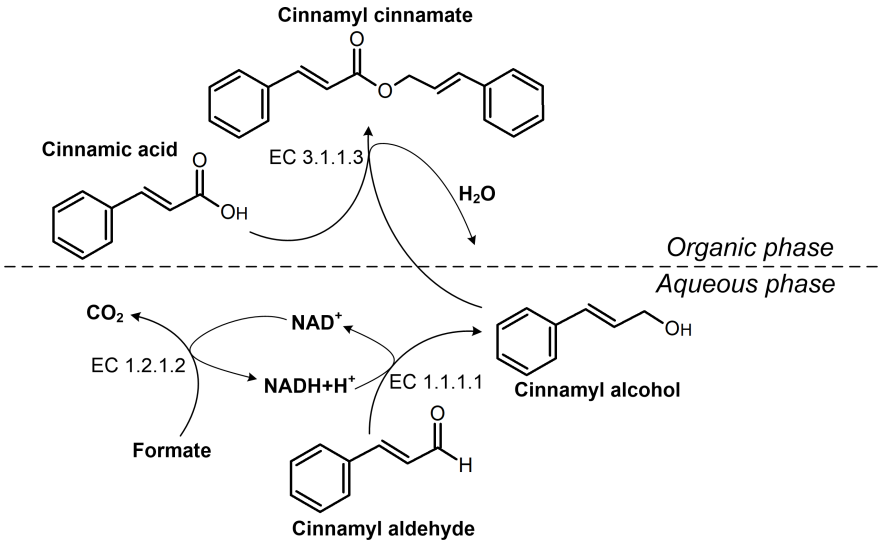

Posted on Authorea 2 Sep 2020 — The copyright holder is the author/funder. All rights reserved. No reuse without permission. — https://doi.org/10.22541/au.159908941.13197198 — This a preprint and has not been peer reviewed. Data may be preliminary.

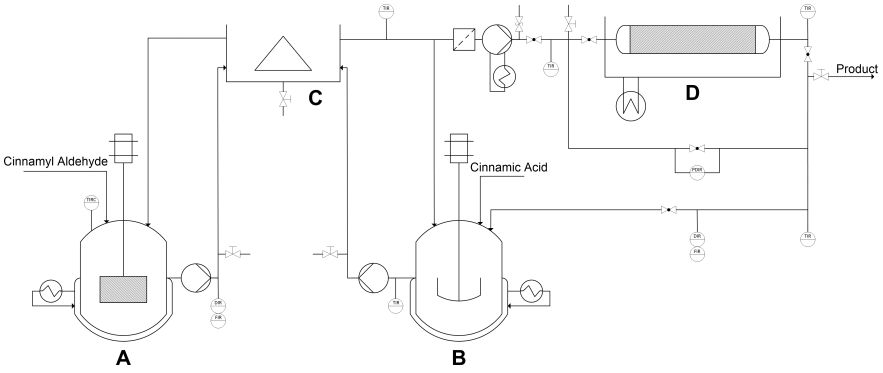

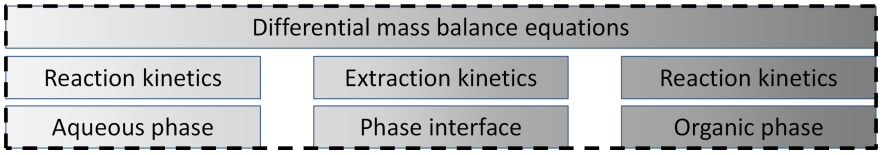

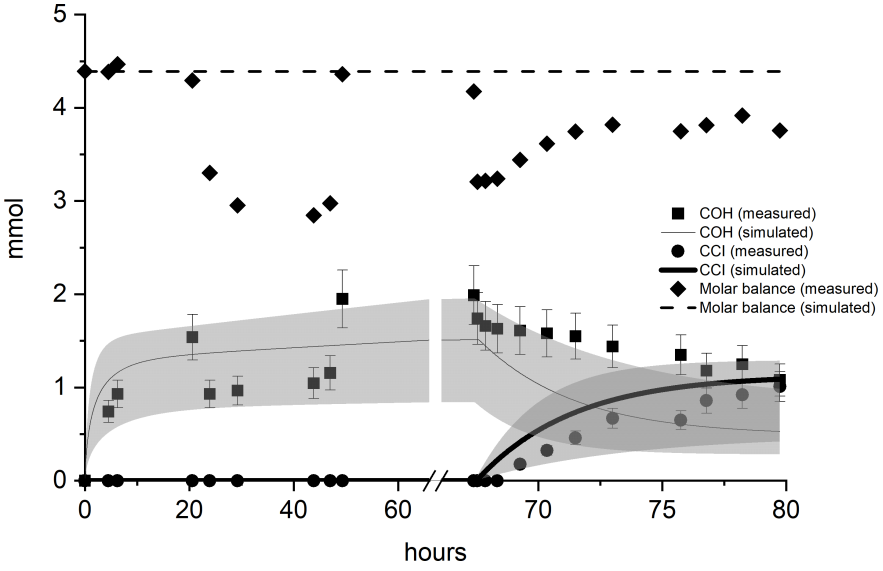

Posted on Authorea 2 Sep 2020 — The copyright holder is the author/funder. All rights reserved. No reuse without permission. — https://doi.org/10.22541/au.159908941.13197198 — This a preprint and has not been peer reviewed. Data may be preliminary.

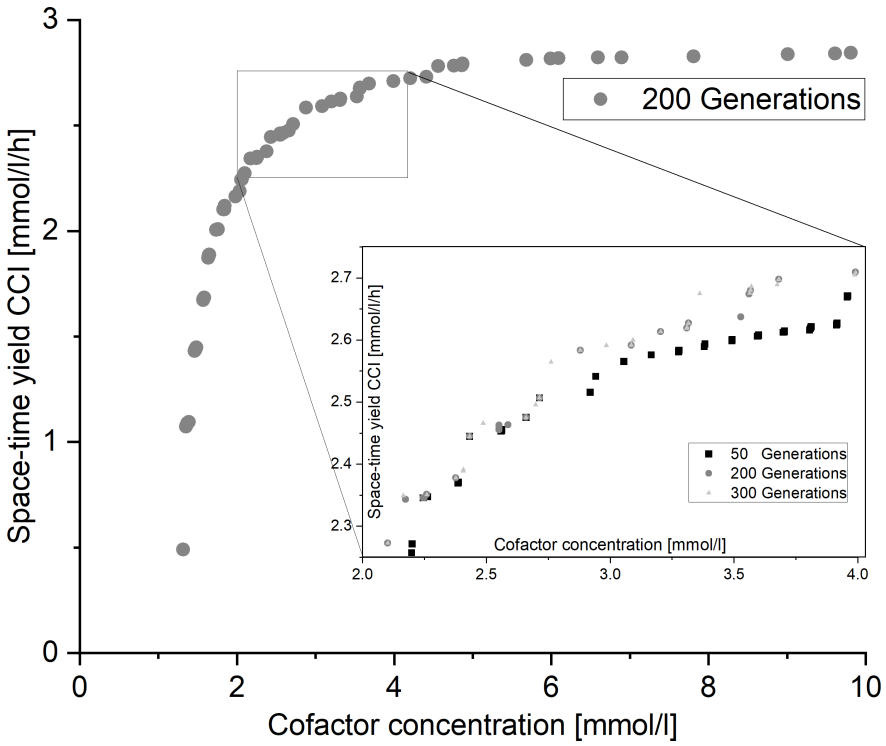

Hosted file

Table 1. Kinetic parameters of the ADH and FDH catalyzed reactions in the aqueous phase..xls available at https://authorea.com/users/354690/articles/478173-multi-enzyme-cascade-reaction-in-a-miniplant-two-phase-system-model-validation-and-mathematical-optimization

Hosted file

Table 2. Partition coefficients of all components in the two phase system..xls available at https://authorea.com/users/354690/articles/478173-multi-enzyme-cascade-reaction-in-a-miniplant-two-phase-system-model-validation-and-mathematical-optimization

Hosted file

Table 3. Kinetic parameters of the lipase catalyzed esterification reaction in the organic xylene phase available at https://authorea.com/users/354690/articles/478173-multi-enzyme-cascade-reaction-in-a-miniplant-two-phase-system-model-validation-and-mathematical-optimization

Hosted file

Table 4. Starting concentrations of educts and CCI yield for the six experiments performed in the minipl available at https://authorea.com/users/354690/articles/478173-multi-enzyme-cascade-reaction-in-a-miniplant-two-phase-system-model-validation-and-mathematical-optimization